Science of the Total Environment 648 (2019) 315–324

Contents lists available at ScienceDirect

Science of the Total Environment

journal homepage: www.elsevier.com/locate/scitotenv

Biophysical effect of conversion from croplands to grasslands in water-limited temperate regions of China

Zhengjia Liu [a,b,*], Yansui Liu [a,b,*], Muhammad Hasan Ali Baig [c]

[a] Institute of Geographic Sciences and Natural Resources Research, Chinese Academy of Sciences, Beijing 100101, China
[b] University of Chinese Academy of Sciences, Beijing 100049, China
[c] Institute of Geo-Information and Earth Observation (IGEO), PMAS Arid Agriculture University, Rawalpindi, Pakistan

HIGHLIGHTS

- Biophysical effect of Conversion from Croplands to Grasslands (C2G) was analyzed.
- C2G resulted in the decrease in net radiation and latent heat.
- C2G led to a cooling effect at the annual scale.
- A warming effect was however found in summer due to more reduction in latent heat.

GRAPHICAL ABSTRACT

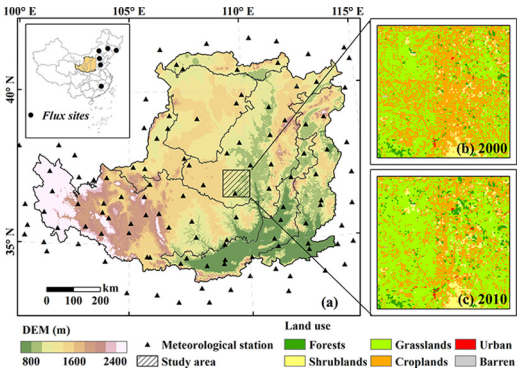

ARTICLE INFO

Article history:
Received 24 May 2018
Received in revised form 8 August 2018
Accepted 9 August 2018
Available online 11 August 2018

Editor: Elena Paoletti

Keywords:
Land use change
Temperature regulation
Net radiation
Latent heat
Water-limited temperate regions

ABSTRACT

The biophysical effect of land use and land cover change (LUCC) on regional climatic regulation is currently of growing interest. However, in water-limited temperate regions, the net biophysical effect of conversion from croplands to grasslands on regional climatic regulation remains poorly understood to date. To answer this concern, a modified land surface model (mEASS) and two different land use scenarios in a typical study area of the Loess Plateau of China were used in this study. We first validated the performances of mEASS model by using observations from six flux tower sites with different land cover and three metrics of the coefficient of determination (R^2), the root mean square error (RMSE) and the difference between the simulated and observed data (bias). Subsequently, the biophysical effect of conversion from croplands to grasslands was investigated. Results indicated that mEASS model could well capture the seasonal dynamics of net radiation and latent heat with high R^2 and lower RMSE and bias at grassland, forest and cropland sites. In the context of semi-arid and semi-humid climatic conditions, conversion from croplands to grasslands caused the cooling effect (-0.3 W/m^2) at the annual scale. Similar cooling effects were found in spring (-0.4 W/m^2), autumn (-0.8 ± 0.1 W/m^2) and winter (-0.9 ± 0.1 W/m^2). The decreased latent heat (inducing warming effects) were completely offset by decreased net radiation (inducing cooling effects), which were responsible for the net cooling effects. However, a warming effect with 1.0 ± 0.1 W/m^2 was observed in summer. This is because that magnitude of decreased latent heat is greater than that of decreased net radiation in summer. These findings will enrich our understanding for the biophysical effect of conversion from croplands to grasslands in water-limited temperate regions.

* Corresponding authors at: Center for Regional Agriculture and Rural Development, Institute of Geographic Sciences and Natural Resources Research, Chinese Academy of Sciences, Beijing 100101, China.
E-mail addresses: liuzj@igsnrr.ac.cn (Z. Liu), liuys@igsnrr.ac.cn (Y. Liu).

https://doi.org/10.1016/j.scitotenv.2018.08.128
0048-9697/

1. Introduction

Anthropogenic land use largely alters the structures and functions of temperate ecosystems, further changes ecosystem services (Anderson-Teixeira et al., 2012; Q. Fu et al., 2017; Ouyang et al., 2016). As an important part of ecosystem services, the biophysical effect of land use and land cover change (LUCC) on regional climatic regulation is currently of growing interest (B. Fu et al., 2017; Q. Fu et al., 2017; Jiang et al., 2016; Reinmann et al., 2016; Schultz et al., 2017). LUCC, by altering the land surface biophysical properties, directly regulates regional climate change. Earlier some studies paid more attention to the biogeochemical effect of LUCC (e.g. carbon dynamics), but neglected the biophysical effect (water and energy regulation) of LUCC (Anderson-Teixeira et al., 2012; Simmons and Matthews, 2016). Recent studies suggest that the biophysical effect of LUCC should be fully considered in the studies of terrestrial ecosystems regulating climate (Ulrich et al., 2016; Zhao et al., 2017; Zhu et al., 2017). Besides, there are some studies reporting that if we neglect the biophysical effect of LUCC, the amplitude of climate change may be largely underestimated in tropical evergreen forests of Amazon and croplands of USA and Brazil, however, overestimated in deciduous forests and evergreen forests of North America (Anderson-Teixeira et al., 2012; Beltrán-Przekurat et al., 2012; Betts et al., 2007; Steyaert and Knox, 2008). Therefore, clarifying the biophysical effect of LUCC is very important for enriching our understanding in the impact of LUCC on regional climate change comprehensively.

In view of the importance of forests for climatic regulation, many of previous studies have paid more attention to the biophysical effects of deforestation and afforestation (Beltrán-Przekurat et al., 2012; Bonan, 2008; Li et al., 2016). For example, Bonan (2008) has reviewed that afforestation and reforestation in tropical regions mitigate climatic warming through evaporative cooling effect, however in boreal regions they enhance climatic warming by lowering albedo and increasing net radiation. Subsequently, some studies further support these findings (Lee et al., 2011; Liao et al., 2018). However, the biophysical effect of LUCC is disputed in temperate ecosystems. A main reason is that water conditions limit the evaporative cooling effect in temperate regions (Betts et al., 2007; Bonan, 2008). Many studies focus on clarifying the biological effect of temperate forests in different climatic regions (Li et al., 2016; Peng et al., 2014; Reinmann et al., 2016). These studies improve our understanding of temperate reforestation and afforestation. It is worth noting that in temperate regions, besides forests, croplands and grasslands are also two crucial ecosystems for human survival and development (J. Liu et al., 2014; Liu et al., 2018a). In order to achieve more crop yield, people early reclaimed swathes of grasslands and forests. In recent decades, some regions have been suffered from serious ecological issues due to unreasonable land use, especially in some temperate regions facing water scarcity (Feng et al., 2016; J. Liu et al., 2014). To recover the function of ecosystems, some ecological engineering were practiced in these fragile ecological zones (Liu et al., 2018a; Ouyang et al., 2016). For example, in the Loess Plateau, the 'Grain for Green' project has been carried out since 1999. By changing regional land use types, this project effectively reduced area of slope cropland and the amount of soil erosion in the Loess Plateau (Feng et al., 2016; Liu et al., 2018a; Wang et al., 2015). Some studies suggest that instead of obtaining huge ecological benefits, large reforestation could potentially aggravate water availability crisis in arid and semi-arid regions, and could further result in more serious ecological damage (Feng et al., 2016; Gao et al., 2014). Another study reports that vegetation expansion in water-limited regions creates potentially conflicting demands for water between ecosystems and humans, and indicates that if regional net primary productivity is far >400 ± 5 gC/m^2/a, humans will suffer from water shortages (Feng et al., 2016). Among ecological engineering, conversion from croplands to grasslands is thus thought of as the best measure for revegetation in water-limited Loess Plateau. However, based on the above mentioned studies in water-limited temperate regions, the net effect of conversion from croplands to grasslands on regional climatic regulation, resulting from the combined positive and negative effects on net radiation and latent heat, remains poorly understood to date.

In recent years, remote sensing techniques and process simulation models are regarded as two main tools for investigating the biophysical effect of LUCC (Beltrán-Przekurat et al., 2012; Bonan, 2008; Li et al., 2016; Peng et al., 2014; Thompson and Paull, 2017; Zhu et al., 2017). The former usually assesses the changes of climatic variables response to LUCC through the space-for-time substitution method (Chen et al., 2017; Peng et al., 2014). These satellite-based methods assume that spatial and temporal variations are equivalent (Pickett, 1989). In contrast, the latter is a main tool for investigating the complex heat interactions between land and atmosphere by setting different LUCC scenarios (Betts, 2000; Bonan et al., 1992; Reinmann et al., 2016). More importantly, the strength of process simulation models is that it can more clearly explain the variation mechanisms of complex processes (Betts et al., 2007; Bonan, 2008; Feddema et al., 2005). In this study, we thus employed a process-based land surface model to investigate the biophysical effect of conversion from croplands to grasslands.

The objectives of this study are: (1) to compute net radiation and latent heat based on different LUCC scenarios; (2) to analyze the biophysical effect of conversion from croplands to grasslands in water-limited mid-latitude regions; and (3) to further clarify potential mechanisms of the biophysical effect. The analyses are based on the assumption that land use change can alter land cover properties (e.g. land surface albedo, leaf area index, and clumping index), and further primarily affect the dynamics of net radiation and latent heat.

2. Data and methods

2.1. Study area

To improve the simulation effectively and clarify the concern of this study clearly, we select the study area with 100 km × 100 km (Fig. 1), given that this region experienced from large-area conversion from croplands to grasslands in the past decade. During the period from 2000 to 2010, land use data indicate that the area of croplands decreased by 16.5% of the study area (J. Liu et al., 2014). Most decreased croplands are replaced by grasslands. Specifically, increased grasslands account for 12.6% of the study area.

The study area is located in the central Loess Plateau, China (36°27′–37°23′N, 108°59′–110°11′E), covering some regions of Ansai, Baota, Yanchang, Qingjian, Yanchuan, Zizhou and Zichang counties. This region has a typical arid, semi-arid and semi-humid continental monsoon climate. Croplands (covering rain-fed spring wheat or spring maize) and grasslands, as two main land use types, both accounted for 87.5% of study area in 2010.

2.2. Meteorological and observed flux data

Daily station-based meteorological data, covering precipitation, air temperature (maximum and minimum), sunshine hour, relative humidity, and wind speed for the period from 1980 to 2012, were collected from the China Meteorological Data Sharing Service (CMA). There is a total of 118 meteorological stations, including 74 meteorological stations in the Loess Plateau and 44 meteorological stations around the Loess Plateau within a range of 10 km. Based on the thin-plate smoothing spline method (ANUSPLIN) and 1 km SRTM digital elevation model (DEM) from SRTM, these above station-based meteorological data were first used for deriving 1 km spatial resolution meteorological datasets (Hutchinson et al., 2009; Liu et al., 2018b). The downward shortwave radiation is a function of latitude, date and sunshine hour (Allen et al., 1998). Then, according to the input requirement of the land surface model used in this study (see Section 2.4), daily interpolated meteorological data were converted to hourly data using the recommended

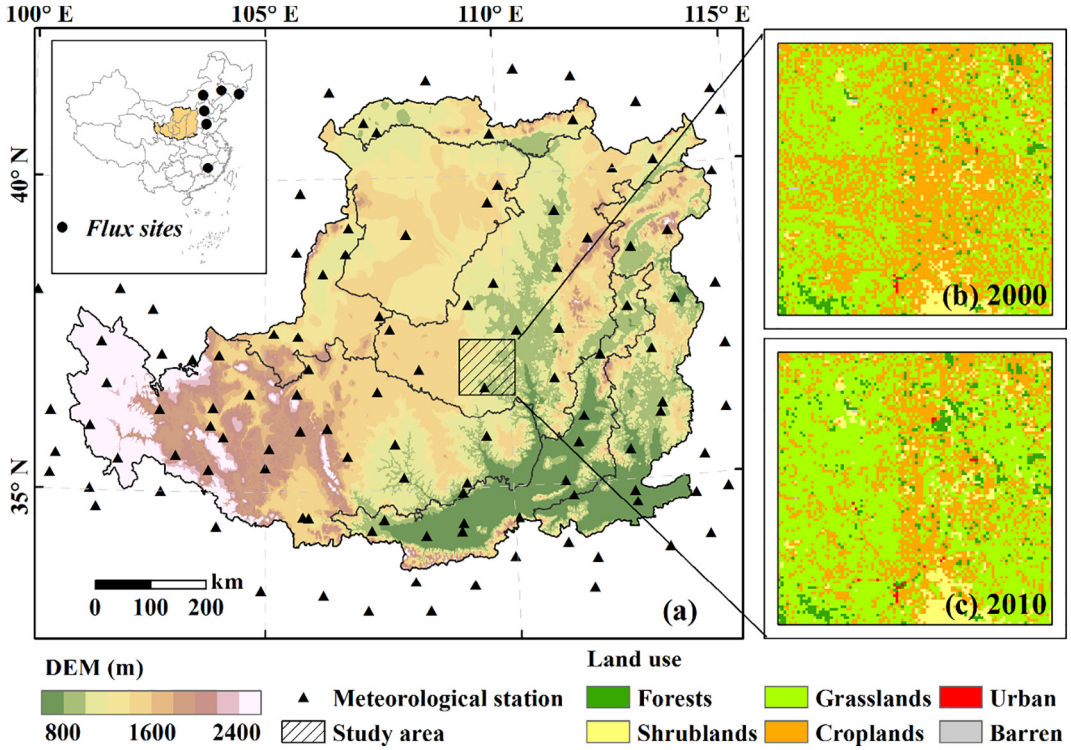

Fig. 1. The location of study area, distribution of digital elevation model (DEM), meteorological stations (a) and land use of study area in 2000 (b) and in 2010 (c). The land use types in study area mainly cover forests, shrublands, grasslands, croplands, urban and built-up (Urban), and barren and sparsely vegetated (Barren).

methods by the previous study of Yan et al. (2014). Specifically, hourly relative humidity, wind speed, and precipitation were linearly interpolated from daily data. Hourly downward shortwave radiation (dsr_h) is a function of the daily downward shortwave radiation (dsr_d) and the theoretical length of daytime (day_{length}).

$$dsr_{hi} = \begin{cases} 0 & (i<b \text{ or } i>c) \\ dsr_d \cdot 11.574 \cdot \sin\left(\dfrac{\pi \cdot (i-(b))}{day_{length}}\right) \Big/ \sin\left(\dfrac{\pi}{24-day_{length}-a}\right) & (b \le i \le c) \end{cases} \quad (1)$$

where, dsr_{hi} is the ith hourly downward shortwave radiation (W/m^2), and i ranges from 0 to 23. The adjusted parameter a is equal to 4.0, $b = 12 - \frac{day_{length}}{2}$ and $c = 12 + \frac{day_{length}}{2}$, respectively. Hourly air temperature (T_h) is a function of daily maximum (T_{max}) and minimum air temperature (T_{min}).

$$T_{hi} = \sin\left(\frac{\pi \cdot i}{12} - \frac{2\pi}{3}\right) \cdot \frac{T_{max} - T_{min}}{2} + \frac{T_{max} + T_{min}}{2} \quad (2)$$

where, T_{hi} is the ith hourly air temperature (°C) and i ranges from 0 to 23.

Half-hourly observed data of flux towers were obtained from six local flux tower sites (Table 1), which cover two grassland sites (Aolinpike site and Xilinguole site), two cropland sites (Tongyu site with spring maize and Yucheng site with the crop rotation of winter wheat and summer maize) and two forest sites (Changbaishan site with mixed forests and Qianyanzhou site with evergreen needleleaf forests) (Z. Liu et al., 2014; Liu et al., 2017). Note that all of these sites observed radiation and latent heat flux records according to ChinaFlux standard (Yu et al., 2006). The half-hourly data were first aggregated into hourly data and then used to validate the performance of land surface model in this study.

Table 1
Brief descriptions of the six flux tower sites in this study. The period of observed flux data used in this study is from January to December of a single year.

Sites	Land use	Latitude/°N	Longitude/°E	Elevation/m	Period
Aolinpike	Grasslands	40.03	116.40	38.5	2012
Xilinguole	Grasslands	43.63	116.70	1100	2005
Tongyu	Croplands	44.20	122.87	184	2003
Yucheng	Croplands	36.95	116.60	28	2005
Changbaishan	Frests	42.40	128.10	738	2005
Qianyanzhou	Forests	26.75	115.67	102	2004

2.3. Satellite-based data and other auxiliary data

Land use data with 1 km spatial resolution in 2000 and 2010 were acquired from the Data Center for Resources and Environmental Sciences, Chinese Academy of Sciences (J. Liu et al., 2014). They were derived from Landsat TM/ETM+ and HJ-1 sensors. The results of field work and random sampling reported that the land use maps were accurate to over 80% at the national scale (J. Liu et al., 2014; Zhang et al., 2014).

Leaf area index (LAI) is a crucial parameter, which plays a crucial role in the interaction between near-surface atmosphere and vegetation by influencing the surface fluxes in the lower boundary layer. The 8-day temporal resolution and 1 km spatial resolution GLASS LAI product in 2000–2012 was collected from the Center for Global Change Data Processing and Analysis of Beijing Normal University. Earlier studies reported that this data had better performances than MODIS LAI (Liang et al., 2013; Xiao et al., 2014). Generally, when land use changes, land cover also changes (Hao et al., 2014; Hao et al., 2015). To perform the process of land cover change in land surface model, we first used the rational equation to develop the DOY-based LAI model. Subsequently, the model along with remote-sensing LAI was used to derive annual LAI dynamics.

$$LAI_{sim_{i,j}} = LAI_{max\_i} \cdot \frac{p_1 + p_2 \cdot j}{1 + p_3 \cdot j + p_4 \cdot j^2} \quad (3)$$

$$LAI_{i,j} = a \cdot LAI_{RS\_j} + b \cdot LAI_{sim\_i,j} \quad (4)$$

where, $LAI_{sim_{i,j}}$ is the simulated LAI at *j*th DOY of *i*th year; LAI_{max_i} is the maximum LAI in *i*th year, which is linearly related with the corresponding annual total precipitation; *j* is DOY; $p_1 \ldots p_4$ are regression parameters; the parameters a and b are both set as 0.5; LAI_{RS_j} is the remote-sensing LAI at *j*th DOY in 2000; and $LAI_{i,j}$ is the simulated LAI at *j*th DOY of *i*th year, which can perform annual LAI dynamics in different land use types and climate change, and is thus finally used to steer land surface model.

Clumping index is also an important structural parameter of plant canopy, which quantifies the level of foliage grouping within distinct canopy structures relative to a random distribution. To minimize the impact of plant canopy structures on radiation absorption, a look-up-table-based clumping index was used in this study. The clumping index values in different land use types referred to previous studies (Chen and Cihlar, 1995; Chen et al., 1999).

The 8-day temporal resolution and 1 km spatial resolution MODIS land surface albedo (V005), including MCD43B3 (data file) and MCD43B2 (quality identification documents), were collected form the Land Processes Distributed Active Archive Center. Based on our previous study in investigating the relationships between land surface albedo and land use types (Liu et al., 2015b), we introduced look-up-table-based land surface albedo in view of snow-free and snow-cover scenarios. Soil data were obtained from the Land-atmosphere Interaction Research Group of Beijing Normal University (Shangguan et al., 2012). Atmospheric carbon dioxide records were collected from air samples at Mauna Loa, Hawaii (Keeling et al., 1995).

2.4. Land surface model

In this study, we employed the Ecosystem Atmosphere Simulation Scheme (EASS), which was developed by Chen et al. (2007). Note that, using observations collected from flux tower stations, we modified some algorithms of net radiation and latent heat of original EASS model according to the objective of this study. Some parameters related to stomatal resistance, aerodynamic resistance and the maximum carboxylation rate were also calibrated (Table 2). The modified model is called mEASS model in the following study. For the sake of simplicity, we only described two key processes of net radiation and latent heat of mEASS model. More detail descriptions of other functions of mEASS model can be found in the previous EASS model (Chen et al., 2007; Chen et al., 2012).

2.4.1. Net radiation

Total net radiation is a function of net shortwave radiation and net longwave radiation, as follows.

$$Rn = Rns + Rnl \quad (5)$$

where, Rn, Rns and Rnl represent total net radiation, net shortwave radiation and net longwave radiation, and their units are W/m^2. In the model, Rns is divided into two major parts of direct and diffuse shortwave radiation (Rns_{dir} and Rns_{dif}), referring to the modified and validated empirical formula of earlier studies (Black et al., 1991; Erbs et al., 1982). The diffuse radiation fraction is calculated using the following function (Chen et al., 2012).

$$\frac{S_{dif}}{S_g} = \begin{cases} 0.943 + 0.734 \cdot R - 4.9 \cdot R^2 + 1.796 \cdot R^3 + 2.508 \cdot R^4 & (R \le 0.8) \\ 0.13 & (R > 0.8) \end{cases} \quad (6)$$

$$R = \frac{S_g}{S_0 \cdot \cos\theta} \quad (7)$$

$$S_{dir} = S_g - S_{dif} \quad (8)$$

where, S_g presents the global solar radiation in W/m^2; R is a ratio between S_g and $S_0 \cdot \cos\theta$, of which S_0 is the solar constant being equal to 1367 W/m^2 and $\cos\theta$ represents the cosine of zenith angle θ; S_{dif} and S_{dir} are the diffuse and direct radiation fractions with the unit of W/m^2, respectively. The two major parts of Rns cover parts of plant canopy (the subscript of pc), under-canopy vegetation (the subscript of uv) and ground (the subscript of g), respectively.

$$Rns = Rns_{dir} + Rns_{dif} \quad (9)$$

$$Rns_{dir} = Rns_{dir\_pc} + Rns_{dir\_uv} + Rns_{dir\_g} \quad (10)$$

$$Rns_{dif} = Rns_{dif\_pc} + Rns_{dif\_uv} + Rns_{dif\_g} \quad (11)$$

Specifically, each part of direct and diffuse shortwave radiation for plant canopy, under-canopy vegetation and ground is calculated using the following equation.

$$Rns_{j\_i} = (1 - \alpha_i) \cdot S_j \cdot f_i \quad (12)$$

where, *i* represents the part of shortwave radiation for plant canopy, under-canopy vegetation or ground; *j* represents direct or diffuse factions of shortwave radiation; α_i is the *i*th part of land surface albedo; f_i is the *i*th part of proportion, ranging from 0 to 1, and largely dependent on LAI; and S_j is the *j*th part of shortwave radiation. Based on flux tower observations, the functions of longwave radiation for each part of longwave radiation in plant canopy, under-canopy vegetation and ground are modified in this study, as follows.

$$Rnl_i = -\varepsilon_i \cdot \frac{\varepsilon_i \sigma (T_i + 237.3)^4 + \varepsilon_a \sigma (T_a + 237.3)^4}{2} \cdot f_i \cdot (0.34 - 0.14\sqrt{e_a}) \cdot \left(1.35 \frac{S_g}{S_{id}} - 0.35\right) \quad (13)$$

$$\varepsilon_a = 1.24 \cdot \sqrt[7]{\frac{e_a}{T_a}} \quad (14)$$

$$e_a = 0.6108 \cdot \exp\left(\frac{17.3 \cdot T_a}{(237.3 + T_a)}\right) \cdot \frac{Rh}{100} \quad (15)$$

where, *i*, f_i and S_g have the same meaning with descriptions of former equations; σ is Stefan-Boltzmann constant being equal to 5.67×10^{-8} $W/m^2/K^4$; T_i is the *i*th part of temperature with the unit of °C; T_a is the air temperature with the unit of °C; S_{id} is an ideal global solar radiation with clear sky (W/m^2); $\frac{S_g}{S_{id}}$ is approximately set as 0.788 referred to flux tower observations; ε_i is the *i*th part of land surface emissivity, of which ε_{cp}, ε_{uv} and ε_{ug} are separately 0.98, 0.98 and 0.95 (Chen and Zhang, 1989); ε_a is a function of air temperature and e_a (Chen et al., 2007), of which e_a is water vapor pressure (mb); and Rh is relative humidity (%).

2.4.2. Latent heat

The hydrological process in the model comprehensively includes evaporation (E_{cp}) and transpiration (TV_{cp}) from plant canopy,

Table 2
Calibrated biophysical parameters used in the model for four main plant functional types.

Parameters/[unit]	Evergreen needleleaf forests	Mixed forests	Croplands	Grasslands
Vcmax/[$\mu mol \cdot m^{-2} \cdot s^{-1}$ at 25 °C]	30	24	45	30
Clumping index/[−]	0.5	0.6	0.9	0.9
Rooting depth/[m]	0.60	0.66	0.25	0.25
Plant height/[m]	15	18	1.2	0.2
Minimum value of stomatal resistant/[$s \cdot m^{-1}$]	150	160	100	100

evaporation (E_{uv}) and transpiration (TV_{uv}) from under-canopy vegetation, evaporation from ground (E_g), and evaporation from rain interception (S_{rain}) or snow interception (S_{snow}). Among them, E_{cp}, TV_{cp}, E_{uv} and TV_{uv} are considered as LE from the vegetation layer (LE_v), and E_g and S_{rain} or S_{snow} are regarded as LE from the soil layer (LE_g). For the sake of simplicity, in the model, evapotranspiration from the vegetation layer is assumed to deplete precipitation interception first, given that the corresponding resistance is relatively less. After the intercepted precipitation has been exhausted by evaporation, transpiration consumes water from soil layers in the root zone (Chen et al., 2007). A six-layer scheme (increases exponentially from the top layer to the sixth layer, equaling to 0.05, 0.1, 0.2, 0.4, 0.8 and 1.6 m, respectively) was used to estimate water transfers through soil profiles and the snowpack (if present). Water movement in each soil layer occurs in the context of saturated and unsaturated conditions (Buckingham, 1907; Chen et al., 2007). In saturated conditions, water movement is mostly horizontal. In unsaturated conditions, water movement is estimated using the modified Darcy's equation by Buckingham (1907). Changes of soil volumetric water content is determined by solving the one-dimensional Richards equation numerically (Richards, 1931).

Specifically, the total latent heat with the unit of W/m^2 is calculated as follows.

$$LE = E_{cp} + TV_{cp} + E_{uv} + TV_{uv} + E_g + S_{rain} + S_{snow} \quad (16)$$

Among them, evaporation calculation refers to the Penman-Monteith equation (Chen et al., 2007).

$$E_i = \frac{\Delta \cdot R_{n\_i} + \rho \cdot C_p \cdot VPD/r_a}{\Delta + \gamma \cdot (1 + r_l/r_a)} \quad (17)$$

where, Δ is slope vapor pressure curve (kPa/°C); R_{n_i} is the ith part of net radiation (W/m^2); ρ is the air density at constant pressure (kg/m^3); C_p is specific heat at constant pressure ($W \cdot s/kg/°C$); VPD is vapor pressure deficit (kPa); r_a is aerodynamic resistance for above-canopy heat and water vapor fluxes (s/m); γ is the psychrometric constant (kPa/°C); and r_l is the stomatal resistance at the leaf level for vegetation or soil resistance for ground (s/m). To improve the performance of plant transpiration estimation, transpiration from sunlit and shaded leaves of plant canopy and under-canopy vegetation are computed, respectively.

$$TV_i = TV_{i\_sunlit} \cdot LAI_{i\_sunlit} + TV_{i\_shaded} \cdot LAI_{i\_shaded} \ (\text{when } M_i = 0) \quad (18)$$

$$LAI_{i\_sunlit} = \begin{cases} 2 \cdot \cos\theta \cdot \left(1 - \exp\left(-0.5 \cdot \Omega \cdot \frac{LAI_i}{\cos\theta}\right)\right) & (cos\theta > 0) \\ 0 & (cos\theta \le 0) \end{cases} \quad (19)$$

$$LAI_{i\_shaded} = LAI_i - LAI_{i\_sunlit} \quad (20)$$

where, i represents plant canopy or under-canopy vegetation; LAI of the sunlit leaf is functions of LAI, the clumping index (Ω) and cosine of zenith angle θ ($\cos\theta$); LAI of the shaded leaf is the remainder of LAI of the sunlit leaf; and M_i is the intercepted precipitation. Besides, intercepted precipitation, including rain and snow, is usually consumed by evaporative heat, and thus plays an important role in evaporation process of plant canopy and under-canopy vegetation. This evaporation is computed by using the following equation.

$$S_i = \min(\lambda_{rain/snow} \cdot S_{i\_p}, \lambda_{rain/snow} \cdot M_i) \quad (21)$$

where, i represents plant canopy or under-canopy vegetation; $\lambda_{rain/snow}$ is latent heat of vaporization and largely dependent on temperature; and S_{i_p} also refers to the Penman-Monteith equation (Chen et al., 2007).

2.5. Design of experiments and statistical analyses

To isolate the biophysical effect of conversion from croplands to grasslands, two experiments were separately performed using same meteorological data, soil data, elevation data and atmospheric carbon dioxide records, but with different land use data and vegetation properties (LAI, clumping index and land surface albedo). Specifically, in the experiment 1 (EXP1) and 2 (EXP2), land use in 2000 and in 2010 along with their corresponding vegetation properties were used to force land surface model, respectively (Table 3 and Fig. 2). The mEASS model was initialized by a spin-up phase to obtain an equilibrium state for plant, soil and atmospheric conditions appropriate to the period of 1980–1989. Therefore, in the following analyses, results for period of 1990–2012 were only used. As energy balance function can be transformed as the following function: $Rn - LE = H + G$, of which H and G are sensible heat flux and ground heat flux. So, in a relative long period, H and G will finally be consumed to heat air temperature of the boundary layer. In this process, land use change, however, can alter land cover properties, e.g. land surface albedo, leaf area index, clumping index, plant height, etc., to more affect net radiation and latent heat. Based on this assumption, this study employed the output results of two experiments for the period of 1990–2012 and the following equation to quantitatively investigate the biophysical effect of land use change.

$$\Delta(Rn - LE) = (Rn_{EXP2} - LE_{EXP2}) - (Rn_{EXP1} - LE_{EXP1}) \quad (22)$$

where, $\Delta(Rn - LE)$ is regarded as the magnitude of the biophysical effect due to land use change in this study. Specifically, if the value of $\Delta(Rn - LE)$ is positive, suggesting that land use change results in the warming effect; conversely, if the value of $\Delta(Rn - LE)$ is negative, suggesting the cooling effect. Rn_{EXP2}, LE_{EXP2}, Rn_{EXP1}, and LE_{EXP1} are the total net radiation and total latent heat from EXP2 and EXP1, respectively.

To evaluate the performance of land surface model, the coefficient of determination (R^2), the root mean square error (RMSE), and the difference between the simulated and observed data (bias) were computed, respectively. The statistical significance is based on the p-value of a two-tailed Student's t-test. In this study, a significant or very significant difference is attained when the observed p-value is <0.05 or 0.01 (the significance level). Conversely, if the p-value is >0.05, the difference is regarded as not significant statistically.

3. Results

In this section, we first validated the performances of mEASS model against site-based observed net radiation and latent heat at six sites. After assuring the performance of model, we used estimated net radiation and latent heat (derived from validated mEASS model in two different land use scenarios) to investigate the impacts of conversion from croplands to grasslands on changes in net radiation and latent heat. Finally, we explained the biophysical effect of conversion from croplands to grasslands in semi-arid and semi-humid mid-latitude regions.

Table 3
A simple description of the experimental design.

Experiment	Changed forcing variables	Unchanged forcing variables
EXP1	Land use in 2000 and the corresponding land surface albedo, clumping index, and LAI in 1980–2012	Meteorological data in 1980–2012, soil data, elevation data and atmospheric carbon dioxide record in 1980–2012
EXP2	Land use in 2010 and the corresponding land surface albedo, clumping index, and LAI in 1980–2012	

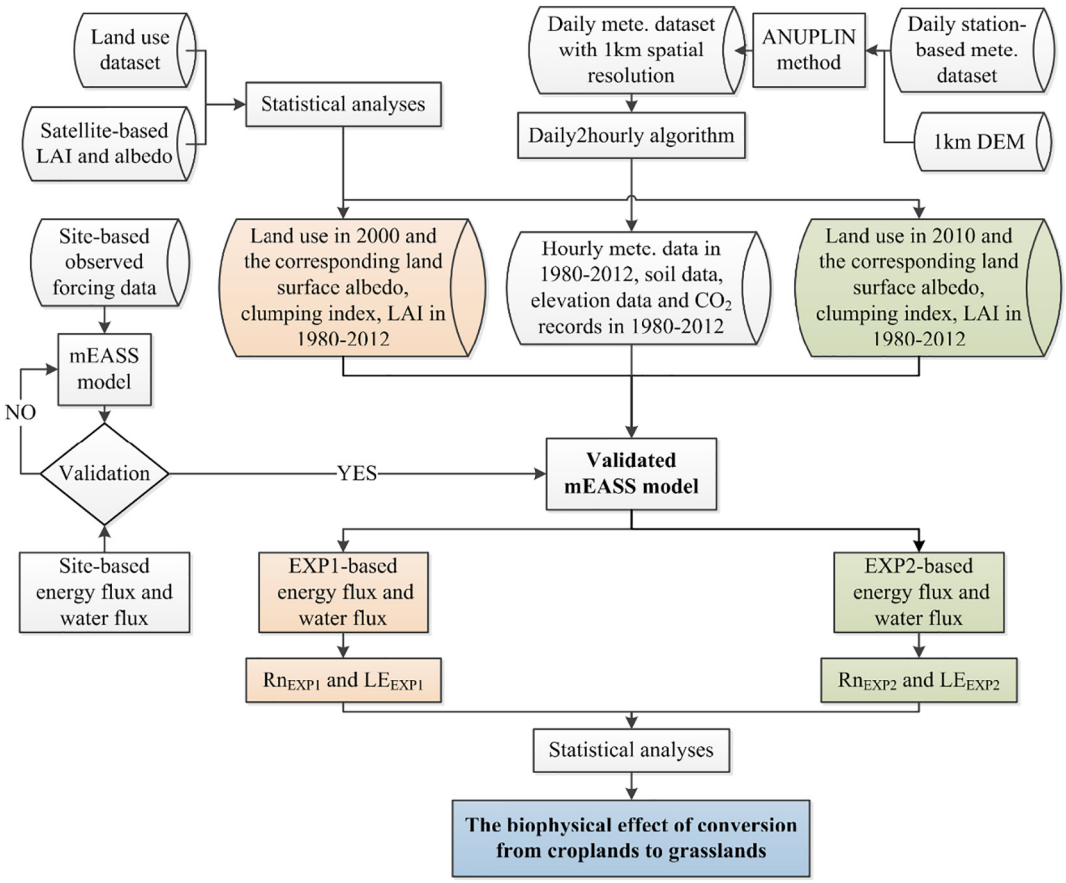

Fig. 2. The workflow of this study.

3.1. Performances of the modified land surface model

Using observed net radiation and latent heat collected from six flux tower sites with different land cover, this study validated the performances of mEASS model (Fig. 3). Validations showed that mEASS model could capture well the seasonal dynamics of net radiation and latent heat in all six flux tower sites. Estimated net radiation usually had better performances than estimated latent heat when we only referred to R^2. R^2 of net radiation ranged from 0.71 to 0.87 ($p < 0.01$). Most R^2 of latent heat were about 0.5–0.6 ($p < 0.01$). A lower R^2 (0.18) was observed in Xilinguole grassland site ($p < 0.01$). In 2005, Xilinguole grassland site suffered from the severe drought event, which could affect the performance of mEASS model to some extent (Fu et al., 2006; Liu et al., 2015a). The phenomenon also reflects the challenge of correctly capturing the severe drought event for current mEASS model. When referring to two metrics of RMSE and bias, we found latent heat generally had relative lower RMSE and bias than corresponding net radiation in all six flux tower sites. For different land cover, lower RMSE and bias of net radiation and latent heat were usually observed in grasslands, followed by forests. In summary, for net radiation prediction and latent heat prediction, mEASS model gave robust performances in grasslands, forests and croplands when we comprehensively considered three metrics of R^2, RMSE and bias.

3.2. Changes of modelled net radiation and latent heat

We found that conversion from croplands to grasslands reduced net radiation (Fig. 4a), and further resulted in the cooling effect when the biophysical effect induced by changes of net radiation were only considered. At the annual scale, net radiation was decreased by 12.2 ± 1.3 W/m^2. Also, the cooling effects were all observed at the seasonal scales. Among them, summer had the strongest cooling effect (−23.4 ± 2.7 W/m^2), followed by spring (−13.2 ± 1.5 W/m^2) and autumn (−8.2 ± 1.0 W/m^2). Winter had the weakest cooling effect (−4.1 ± 0.5 W/m^2).

At the annual and seasonal scales, conversion from croplands to grasslands resulted in the decrease of latent heat (Fig. 4b), but it resulted in the warming effect if only the biophysical effect induced by changes of latent heat were considered. At the annual scale, latent heat decreased by 11.9 ± 1.4 W/m^2. At the seasonal scales, summer had the strongest warming effect (−24.4 ± 3.2 W/m^2), followed by spring (−12.8 ± 2.3 W/m^2) and autumn (−7.4 ± 1.2 W/m^2). Winter had the weakest warming effect (−3.2 ± 0.4 W/m^2).

3.3. Net biophysical effect of conversion from croplands to grasslands

Fig. 5 shows that conversion from croplands to grasslands led to the cooling effect with −0.3 W/m^2 at the annual scale. This is mainly because as compared to the annual decrease in latent heat, annual decrease in net radiation contributed more to the cooling effect. Similar phenomena were also observed in spring, autumn and winter. The stronger cooling effect was found in winter (−0.9 ± 0.1 W/m^2), followed by autumn (−0.8 ± 0.1 W/m^2). However, a warming effect with 1.0 ± 0.1 W/m^2 was found in summer. The amount of decreased latent heat in summer exceeded the decrease in net radiation, resulting in a warming effect.

4. Discussion

The study of Betts et al. (2007) stated that many consequences of climate change for human society would depend more on regional-scale

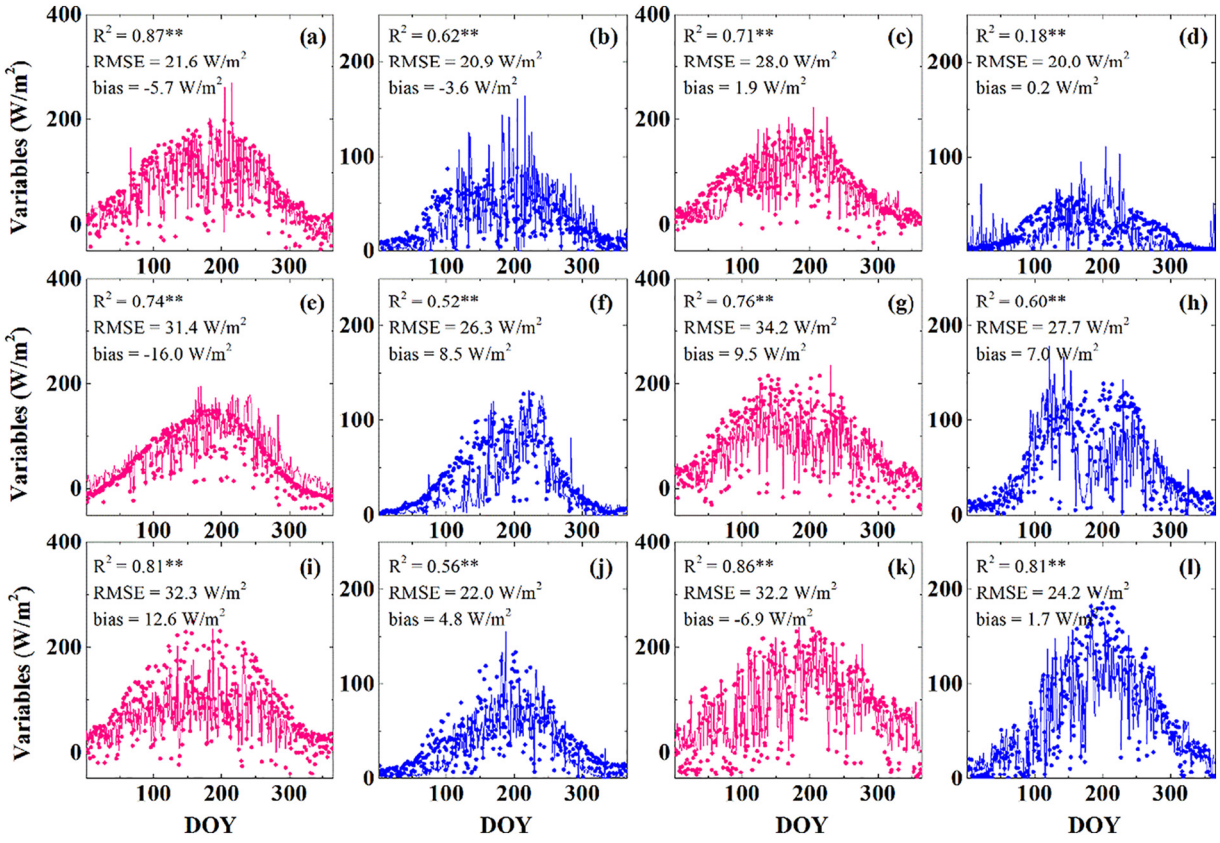

Fig. 3. Validations of net radiation (pink color) and latent heat (blue color) derived from modified land surface model against observed flux tower data (solid line). The top row shows the performances in grasslands (a and b in Aolinpike site, and c and d in Xilinguole site); the middle row shows the performances in croplands (e and f in Tongyu site, and g and h in Yucheng site); and the bottom row shows the performances in forests (i and j in Changbaishan site, and k and l in Qianyanzhou site). The symbol ** represents the significance at the 0.01 statistical level ($p < 0.01$).

changes than global averages, thus global averaged energy changes might be less useful than information from regional-scale changes (Betts et al., 2007; Bonan, 2008; Bonan et al., 1992). Our study highlights the importance of regional-scale researches, and our findings indicate that conversion form croplands to grasslands has led to complex interactions between vegetation and near-surface energy fluxes by modifying the biophysical and physiological properties of land cover. Unlike previous studies which pay more attention to the biophysical effect of afforestation, reforestation, and the shift from grasslands/forests/bare land to croplands (Betts et al., 2007; Li et al., 2016; Peng et al., 2014; Schultz et al., 2017; Ulrich et al., 2016), our study focuses on the biophysical effect of conversion from croplands to grasslands in water-limited regions of China. A main reason of selecting the topic is that in water-limited regions, conversion from croplands to grasslands is generally thought of as the best measure for revegetation among ecological engineering in view of its comprehensive ecosystem services in ecological restoration, soil conservation and runoff regulation.

In this study, conversion from croplands to grasslands exerts a cooling effect at the annual scale, but the result conflicts with

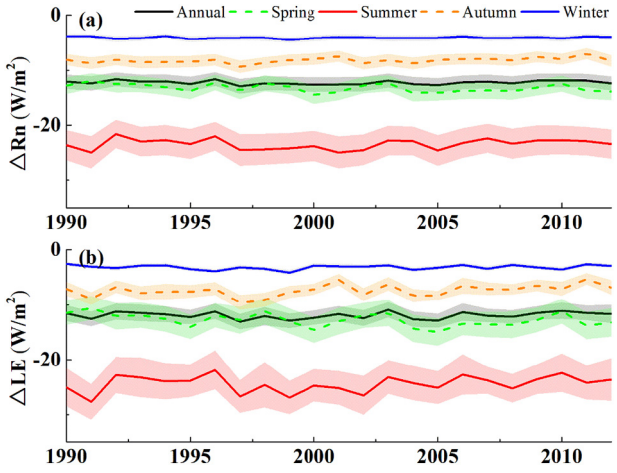

Fig. 4. Interannual variations of differences in net radiation (ΔRn, a) and latent heat (ΔLE, b) at the annual and seasonal scales. Solid/dashed lines and shadow zones represent the averaged values and the corresponding standard deviation of all pixels of conversion form croplands to grasslands in entire study area, respectively.

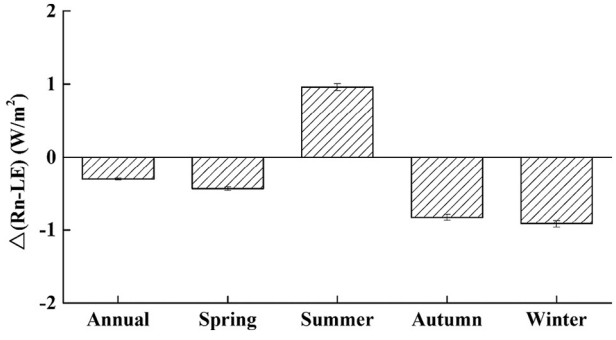

Fig. 5. The net biophysical effect of conversion from croplands to grasslands (Δ(Rn-LE)) at the annual and seasonal scales. Error bars represent 1 standard error. The negative value of Δ(Rn-LE) represents the cooling effect, and the positive value of Δ(Rn-LE) represents the warming effect.

annual warming trend in our region in fact. This is likely because that the cooling effect induced by conversion form croplands to grasslands is relatively weaker than annual warming magnitude in our region (B. Fu et al., 2017), thus conversion form croplands to grasslands in this region only contributes to a reduction in the rate of climate warming. However, if we neglect the cooling effect induced by conversion form croplands to grasslands, climate warming in this region might have been greater than that at the present day. Besides, note that this study considers the changes of land cover. A precipitation-based function is used to regulate changes of LAI, which ensures dynamics of land cover change with climate change. This is different from some earlier studies which fixed LAI as a specific parameter (Betts et al., 2007; Trail et al., 2013). Radiative (via changes in land surface albedo) and non-radiative forcing (via changes in latent heat fluxes) are two main processes that determine the impacts of LUCC on near-surface climate (Beltrán-Przekurat et al., 2012; Betts et al., 2007; Lawrence and Chase, 2010; Pielke et al., 2002). Dynamic LAI is of importance for accurate estimations of latent heat fluxes, and is thus helpful for improving our understanding of two-way interactions between vegetation and atmosphere (Beltrán-Przekurat et al., 2012). In agreement with other studies, our findings underscore the importance of considering plant physiological processes when evaluating the biophysical effect of LUCC (Beltrán-Przekurat et al., 2012; Eastman et al., 2001; Feddema et al., 2005; Thompson and Paull, 2017; Yan et al., 2014).

In regional interpolation, previous some studies usually used Kriging or inverse-distance weighting methods without considering the effect of DEM. These traditional methods of interpolation often perform well over regions with lower elevation or relatively covered by dense stations (Yuan et al., 2014; Yue et al., 2016). However, in complex terrain, many studies have reported that AUNSPIN method we used in this study shows more spatially explicit patterns due to considering the impacts of DEM on climatic variables (Hutchinson et al., 2009; Liu et al., 2018b).

In the following sections, we will discuss in detail the potential mechanisms and reasons of the biophysical effect of conversion from croplands to grasslands.

Conversion from croplands to grassland reduces the net radiation (ΔRn) by 12.2 ± 0.3 W/m^2 at the annual scale (Fig. 6), of which 89% corresponds to changes in net shortwave radiation (ΔRns) and 11% is due to changes in net longwave radiation (ΔRnl). The results suggest that ΔRns play major roles in ΔRn. Also, they potentially highlight the key role of land surface albedo in view of its importance in regulating ΔRns. Conversion from croplands to grasslands increases regional vegetation cover and LAI. Our results also find that annual net radiation from the vegetation layer (ΔRn_v) increases by 3.2 ± 0.2 W/m^2. Meanwhile, because the ratio between net radiation from the soil layer and total net radiation in croplands is usually greater than that in grasslands, increased fraction of vegetation cover induced by conversion from croplands to grasslands thus largely reduces the magnitude of net radiation from the soil layer (ΔRn_g, being −15.5 ± 0.6 W/m^2). At the seasonal scales, we find that vegetation growth makes the amounts of ΔRn_v gradually increased (4.6 ± 0.2 W/m^2 in spring and 9.6 ± 0.8 W/m^2 in summer). Compared to croplands, more advanced green-up date and natural growth in grasslands may be responsible for positive values of ΔRn_v. Gradually increased phenomena are also observed in ΔRn_g (−17.8 ± 1.2 W/m^2 in spring and −33.0 ± 1.6 W/m^2 in summer). In autumn and winter, values of ΔRn_v are negative or closer to zero. This is mainly because that grasslands have much earlier autumn phenology relative to croplands. However, after harvesting in croplands, the value of ΔRn_v is much closer to zero as ΔRn_v of winter showed.

From spring to summer, the amounts of ΔRns and ΔRnl gradually increase mainly due to differences in changes of land surface albedo, land surface temperature and land surface emissivity as well as melting snow in croplands and grasslands. The largest values of ΔRns and ΔRnl are found in summer (−20.5 ± 0.9 W/m^2 and 2.9 ± 0.2 W/m^2, respectively). In contrast, amounts of ΔRns and ΔRnl in the second half of the year are less than those in the first half of the year. Yet, values of ΔRns in autumn and winter are still negative due to the differences of land surface albedo in croplands and grasslands. Note that ΔRns in autumn and winter account for over 90% of ΔRn.

Overall, increased vegetation cover and LAI make ΔRn_v positive, but reduced ΔRn_g have larger amounts than ΔRn_v. Therefore, ΔRn decrease induced by conversion from croplands to grasslands is more controlled by decreased ΔRn_g. Besides, in the process of conversion from croplands to grasslands, changes of land surface albedo decreases net shortwave radiation, which is more responsible for the decrease in ΔRn.

Conversion from croplands to grasslands leads to latent heat decrease (Fig. 7). Our results find that changes of latent heat (ΔLE) are mainly controlled by changes of latent heat from the soil layer (ΔLE_g). Conversion from croplands to grasslands increased the fraction of vegetation cover and regional LAI, and decreased the area of bare soil. At the annual scale, the values of ΔLE, ΔLE_v and ΔLE_g are −11.9 ± 0.6 W/m^2, 0.1 ± 0.2 W/m^2 and −12.0 ± 0.6 W/m^2, respectively. The positive values of ΔLE_v are observed in spring (0.8 ± 0.3 W/m^2) and summer (0.8 ± 0.8 W/m^2). Compared to croplands, more advanced spring phenology and positive ΔRn_v in grasslands may be responsible for positive values of ΔLE_v. However, a positive value of ΔLE_v is found in autumn (−1.1 ± 0.3 W/m^2). Compared to grasslands, later phenology and growth for crop could be responsible for the above phenomenon. At the annual and seasonal scales, all values of ΔLE_g decrease. The largest decreased amount of ΔLE_g is observed in summer (−25.1 ± 1.5 W/m^2), followed by spring (−13.6 ± 1.4 W/m^2) and autumn (−6.3 ± 0.8 W/m^2).

Overall, by mainly decreasing latent heat from the soil layer, conversion from croplands to grasslands reduced regional latent heat. Although the increased fraction of vegetation cover and LAI result in values of ΔLE_v, weaker increase in latent heat contributes little to changes of total latent heat.

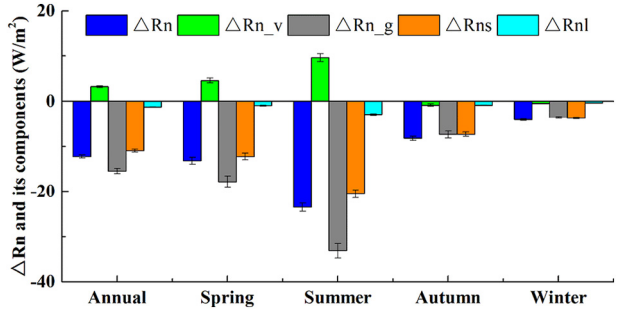

Fig. 6. Changes in difference of net radiation (ΔRn) and its main components. Among them, ΔRn_v changes as difference of net radiation from the vegetation layer, ΔRn_g changes as difference of net radiation from the soil layer. ΔRns and ΔRnl are changes in differences of net shortwave radiation and net longwave radiation, respectively. Vertical thin bars represent standard errors.

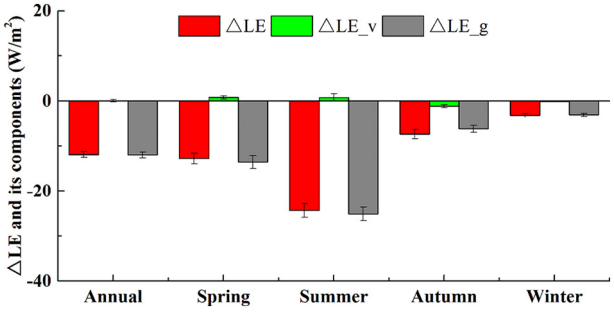

Fig. 7. Changes in difference of latent heat (ΔLE) and its main components. Among them, ΔLE_v changes as difference of latent heat from the vegetation layer, ΔLE_g changes as difference of latent heat from the soil layer.

5. Conclusions

To clarify the biophysical effect of conversion form croplands to grasslands in water-limited temperate regions, two different experiments were separately simulated based on a well-performing land surface model, the modified Ecosystem Atmosphere Simulation Scheme (mEASS). In our experiments, we used land use maps of two different periods of 2000 and 2010 and their corresponding vegetation properties (land surface albedo, leaf area index and clumping index), while the same meteorological data and other auxiliary data was used. Our results showed that a net cooling effect with −0.3 W/m^2 was observed at the annual scale. Similarly, the cooling effect was also found in spring, autumn and winter, while a net warming effect with 1.0 W/m^2 was presented in summer. Changes in net shortwave radiation and latent heat from the soil layer were directly responsible for the above phenomena. These findings will enrich our understanding of how does conversion from croplands to grasslands in semi-arid and semi-humid temperate regions regulate regional climate.

Acknowledgements

We appreciate the original contribution for the development of Ecosystem Atmosphere Simulation Scheme for Prof. Chen's group. Also we sincerely appreciate three anonymous reviewers, editor and my advisors for their valuable suggestions and comments, which improve this manuscript. This study is funded by the National Natural Science Foundation of China (Grant No. 41601582), the National Key Research and Development Program of China (Grant No. 2017YFC0504701) and the Start-up Research Program of IGSNRR funding to Z. Liu.

References

Allen, R.G., Pereira, L.S., Raes, D., Smith, M., 1998. Crop evapotranspiration: guidelines for computing crop water requirements. FAO Irrigation and Drainage Paper: M-56.
Anderson-Teixeira, K.J., Snyder, P.K., Twine, T.E., Cuadra, S.V., Costa, M.H., DeLucia, E.H., 2012. Climate-regulation services of natural and agricultural ecoregions of the Americas. Nat. Clim. Chang. 2 (3), 177–181.
Beltrán-Przekurat, A., Pielke Sr., R.A., Eastman, J.L., Coughenour, M.B., 2012. Modelling the effects of land-use/land-cover changes on the near-surface atmosphere in southern South America. Int. J. Climatol. 32 (32), 1206–1225.
Betts, R.A., 2000. Offset of the potential carbon sink from boreal forestation by decreases in surface albedo. Nature 408 (6809), 187–190.
Betts, R.A., Falloon, P.D., Goldewijk, K.K., Ramankutty, N., 2007. Biogeophysical effects of land use on climate: model simulations of radiative forcing and large-scale temperature change. Agric. For. Meteorol. 142 (2–4), 216–233.
Black, T.A., Chen, J.-M., Lee, X., Sagar, R.M., 1991. Characteristics of shortwave and longwave irradiances under a Douglas-fir forest stand. Can. J. For. Res. 21 (7), 1020–1028.
Bonan, G.B., 2008. Forests and climate change: forcings, feedbacks, and the climate benefits of forests. Science 320 (5882), 1444–1449.
Bonan, G.B., Pollard, D., Thompson, S.L., 1992. Effects of boreal forest vegetation on global climate. Nature 359, 716.
Buckingham, E., 1907. Studies on the Movement of Soil Moisture. USDA Bureau of Soils, Washington, DC, p. 38.
Chen, J.M., Cihlar, J., 1995. Quantifying the effect of canopy architecture on optical measurements of leaf area index using two gap size analysis methods. IEEE Trans. Geosci. Remote Sens. 33 (3), 777–787.
Chen, J.-M., Zhang, R.-H., 1989. Studies on the measurements of crop emissivity and sky temperature. Agric. For. Meteorol. 49 (1), 23–34.
Chen, J.M., Liu, J., Cihlar, J., Goulden, M.L., 1999. Daily canopy photosynthesis model through temporal and spatial scaling for remote sensing applications. Ecol. Model. 124 (2–3), 99–119.
Chen, B., Chen, J.M., Ju, W., 2007. Remote sensing-based ecosystem–atmosphere simulation scheme (EASS)—model formulation and test with multiple-year data. Ecol. Model. 209 (2–4), 277–300.
Chen, J.M., Mo, G., Pisek, J., Liu, J., Deng, F., Ishizawa, M., Chan, D., 2012. Effects of foliage clumping on the estimation of global terrestrial gross primary productivity. Glob. Biogeochem. Cycles 26 (1), GB1019.
Chen, G., Wang, M., Liu, Z., Chi, W., 2017. The biogeophysical effects of revegetation around mining areas: a case study of Dongsheng mining areas in Inner Mongolia. Sustainability 9 (4), 628.
Eastman, Joseph L., Coughenour, Michael B., Pielke, Roger A., 2001. The regional effects of CO_2 and landscape change using a coupled plant and meteorological model. Glob. Chang. Biol. 7 (7), 797–815.
Erbs, D.G., Klein, S.A., Duffie, J.A., 1982. Estimation of the diffuse radiation fraction for hourly, daily and monthly-average global radiation. Sol. Energy 28 (4), 293–302.
Feddema, J.J., Oleson, K.W., Bonan, G.B., Mearns, L.O., Buja, L.E., Meehl, G.A., Washington, W.M., 2005. The importance of land-cover change in simulating future climates. Science 310 (5754), 1674–1678.
Feng, X., Fu, B., Piao, S., Wang, S., Ciais, P., Zeng, Z., Lü, Y., Zeng, Y., Li, Y., Jiang, X., Wu, B., 2016. Revegetation in China's Loess Plateau is approaching sustainable water resource limits. Nat. Clim. Chang. 6, 1019.
Fu, Y., Yu, G., Sun, X., Li, Y., Wen, X., Zhang, L., Li, Z., Zhao, L., Hao, Y., 2006. Depression of net ecosystem CO_2 exchange in semi-arid *Leymus chinensis* steppe and alpine shrub. Agric. For. Meteorol. 137 (3–4), 234–244.
Fu, B., Wang, S., Liu, Y., Liu, J., Liang, W., Miao, C., 2017. Hydrogeomorphic ecosystem responses to natural and anthropogenic changes in the Loess Plateau of China. Annu. Rev. Earth Planet. Sci. 45 (1), 223–243.
Fu, Q., Li, B., Hou, Y., Bi, X., Zhang, X., 2017. Effects of land use and climate change on ecosystem services in Central Asia's arid regions: a case study in Altay Prefecture, China. Sci. Total Environ. 607-608, 633–646.
Gao, Y., Zhu, X., Yu, G., He, N., Wang, Q., Tian, J., 2014. Water use efficiency threshold for terrestrial ecosystem carbon sequestration in China under afforestation. Agric. For. Meteorol. 195-196, 32–37.
Hao, P., Wang, L., Niu, Z., Aablikim, A., Huang, N., Xu, S., Chen, F., 2014. The potential of time series merged from Landsat-5 TM and HJ-1 CCD for crop classification: a case study for Bole and Manas Counties in Xinjiang, China. Remote Sens. 6 (8), 7610.
Hao, P., Zhan, Y., Wang, L., Niu, Z., Shakir, M., 2015. Feature selection of time series MODIS data for early crop classification using random forest: a case study in Kansas, USA. Remote Sens. 7 (5), 5347.
Hutchinson, M.F., McKenney, D.W., Lawrence, K., Pedlar, J.H., Hopkinson, R.F., Milewska, E., Papadopol, P., 2009. Development and testing of Canada-wide interpolated spatial models of daily minimum-maximum temperature and precipitation for 1961–2003. J. Appl. Meteorol. Climatol. 48 (4), 725–741.
Jiang, C., Li, D., Wang, D., Zhang, L., 2016. Quantification and assessment of changes in ecosystem service in the Three-River Headwaters Region, China as a result of climate variability and land cover change. Ecol. Indic. 66, 199–211.
Keeling, C.D., Whorf, T.P., Wahlen, M., van der Plichtt, J., 1995. Interannual extremes in the rate of rise of atmospheric carbon dioxide since 1980. Nature 375, 666.
Lawrence, P.J., Chase, T.N., 2010. Investigating the climate impacts of global land cover change in the community climate system model. Int. J. Climatol. 30 (13), 2066–2087.
Lee, X., Goulden, M.L., Hollinger, D.Y., Barr, A., Black, T.A., Bohrer, G., Bracho, R., Drake, B., Goldstein, A., Gu, L., Katul, G., Kolb, T., Law, B.E., Margolis, H., Meyers, T., Monson, R., Munger, W., Oren, R., Paw, U.K.T., Richardson, A.D., Schmid, H.P., Staebler, R., Wofsy, S., Zhao, L., 2011. Observed increase in local cooling effect of deforestation at higher latitudes. Nature 479, 384.
Li, Y., Zhao, M., Mildrexler, D.J., Motesharrei, S., Mu, Q., Kalnay, E., Zhao, F., Li, S., Wang, K., 2016. Potential and actual impacts of deforestation and afforestation on land surface temperature. J. Geophys. Res. 121 (24), 14,372–14,386.
Liang, S., Zhao, X., Liu, S., Yuan, W., Cheng, X., Xiao, Z., Zhang, X., Liu, Q., Cheng, J., Tang, H., 2013. A long-term global land surface satellite (GLASS) data-set for environmental studies. Int. J. Digital Earth 6 (sup1), 5–33.
Liao, W., Rigden, A.J., Li, D., 2018. Attribution of local temperature response to deforestation. J. Geophys. Res. 123 (5), 1572–1587.
Liu, J., Kuang, W., Zhang, Z., Xu, X., Qin, Y., Ning, J., Zhou, W., Zhang, S., Li, R., Yan, C., Wu, S., Shi, X., Jiang, N., Yu, D., Pan, X., Chi, W., 2014. Spatiotemporal characteristics, patterns, and causes of land-use changes in China since the late 1980s. J. Geogr. Sci. 24 (2), 195–210.
Liu, Z., Wang, L., Wang, S., 2014. Comparison of different GPP models in China using MODIS image and ChinaFLUX data. Remote Sens. 6 (10), 10215–10231.
Liu, Z., Shao, Q., Liu, J., 2015a. The performances of MODIS-GPP and -ET products in China and their sensitivity to input data (FPAR/LAI). Remote Sens. 7 (1), 135–152.
Liu, Z., Shao, Q., Tao, J., Chi, W., 2015b. Intra-annual variability of satellite observed surface albedo associated with typical land cover types in China. J. Geogr. Sci. 25 (1), 35–44.
Liu, Z., Wu, C., Peng, D., Wang, S., Gonsamo, A., Fang, B., Yuan, W., 2017. Improved modeling of gross primary production from a better representation of photosynthetic components in vegetation canopy. Agric. For. Meteorol. 233, 222–234.
Liu, Z., Liu, Y., Li, Y., 2018a. Anthropogenic contributions dominate trends of vegetation cover change over the farming-pastoral ecotone of northern China. Ecol. Indic. 95 (1), 370–378.
Liu, Z., Liu, Y., Wang, S., Yang, X., Wang, L., Baig, M.H.A., Chi, W., Wang, Z., 2018b. Evaluation of spatial and temporal performances of ERA-interim precipitation and temperature in Mainland China. J. Clim. 31 (11), 4347–4365.
Ouyang, Z., Zheng, H., Xiao, Y., Polasky, S., Liu, J., Xu, W., Wang, Q., Zhang, L., Xiao, Y., Rao, E., 2016. Improvements in ecosystem services from investments in natural capital. Science 352 (6292), 1455.
Peng, S., Piao, S., Zeng, Z., Ciais, P., Zhou, L., Li, L.Z.X., Myneni, R.B., Yin, Y., Zeng, H., 2014. Afforestation in China cools local land surface temperature. Proc. Natl. Acad. Sci. U. S. A. 111 (8), 2915–2919.
Pickett, S.T.A., 1989. Space-for-time substitution as an alternative to long-term studies. In: Likens, G.E. (Ed.), Long-term Studies in Ecology: Approaches and Alternatives. Springer New York, New York, NY, pp. 110–135.
Pielke Sr., R.A., Marland, G., Betts, R.A., Chase, T.N., Eastman, J.L., Niles, J.O., Niyogi, D.D., Running, S.W., 2002. The influence of land-use change and landscape dynamics on the climate system: relevance to climate-change policy beyond the radiative effect of greenhouse gases. Philos. Transact. A Math. Phys. Eng. Sci. 360 (1797), 1705–1719.
Reinmann, A.B., Hutyra, L.R., Trlica, A., Olofsson, P., 2016. Assessing the global warming potential of human settlement expansion in a mesic temperate landscape from 2005 to 2050. Sci. Total Environ. 545-546, 512–524.
Richards, L., 1931. Capillary conduction of liquids through porous mediums. J. Appl. Phys. 1, 318–333.

Schultz, N.M., Lawrence, P.J., Lee, X., 2017. Global satellite data highlights the diurnal asymmetry of the surface temperature response to deforestation. J. Geophys. Res. 122 (4), 903–917.
Shangguan, W., Dai, Y., Liu, B., Ye, A., Yuan, H., 2012. A soil particle-size distribution dataset for regional land and climate modelling in China. Geoderma 171–172 (0), 85–91.
Simmons, C.T., Matthews, H.D., 2016. Assessing the implications of human land-use change for the transient climate response to cumulative carbon emissions. Environ. Res. Lett. 11 (3), 035001.
Steyaert, L.T., Knox, R.G., 2008. Reconstructed historical land cover and biophysical parameters for studies of land-atmosphere interactions within the eastern United States. J. Geophys. Res. 113 (D2), D02101.
Thompson, J.A., Paull, D.J., 2017. Assessing spatial and temporal patterns in land surface phenology for the Australian Alps (2000–2014). Remote Sens. Environ. 199, 1–13.
Trail, M., Tsimpidi, A.P., Liu, P., Tsigaridis, K., Hu, Y., Nenes, A., Stone, B., Russell, A.G., 2013. Potential impact of land use change on future regional climate in the Southeastern US: reforestation and cropland conversion. J. Geophys. Res. 118 (20), 11577–11588.
Ulrich, K., Florian, H., Miodrag, S., Benjamin Leon, B., Elmar, K., Hermann, L.-C., Alexander, P., 2016. Afforestation to mitigate climate change: impacts on food prices under consideration of albedo effects. Environ. Res. Lett. 11 (8), 085001.
Wang, S., Fu, B., Piao, S., Lü, Y., Ciais, P., Feng, X., Wang, Y., 2015. Reduced sediment transport in the Yellow River due to anthropogenic changes. Nat. Geosci. 9, 38.
Xiao, Z., Liang, S., Wang, J., Chen, P., Yin, X., Zhang, L., Song, J., 2014. Use of general regression neural networks for generating the GLASS leaf area index product from time-series MODIS surface reflectance. IEEE Trans. Geosci. Remote Sens. 52 (1), 209–223.
Yan, J.W., Liu, J.Y., Chen, B.Z., Feng, M., Fang, S.F., Xu, G., Zhang, H.F., Che, M.L., Liang, W., Hu, Y.F., Kuang, W.H., Wang, H.M., 2014. Changes in the land surface energy budget in eastern China over the past three decades: contributions of land-cover change and climate change. J. Clim. 27 (24), 9233–9252.
Yu, G., Wen, X., Sun, X., Tanner, B.D., Lee, X., Chen, J., 2006. Overview of ChinaFLUX and evaluation of its eddy covariance measurement. Agric. For. Meteorol. 137 (3), 125–137.
Yuan, W., Xu, B., Chen, Z., Xia, J., Xu, W., Chen, Y., Wu, X., Fu, Y., 2014. Validation of China-wide interpolated daily climate variables from 1960 to 2011. Theor. Appl. Climatol. 119 (3–4), 689–700.
Yue, T., Zhao, N., Fan, Z., Li, J., Chen, C., Lu, Y., Wang, C., Xu, B., Wilson, J., 2016. CMIP5 downscaling and its uncertainty in China. Glob. Planet. Chang. 146, 30–37.
Zhang, Z., Wang, X., Zhao, X., Liu, B., Yi, L., Zuo, L., Wen, Q., Liu, F., Xu, J., Hu, S., 2014. A 2010 update of National Land Use/Cover Database of China at 1:100000 scale using medium spatial resolution satellite images. Remote Sens. Environ. 149, 142–154.
Zhao, W., Hu, Z., Li, S., Guo, Q., Liu, Z., Zhang, L., 2017. Comparison of surface energy budgets and feedbacks to microclimate among different land use types in an agro-pastoral ecotone of northern China. Sci. Total Environ. 599–600, 891–898.
Zhu, P., Zhuang, Q., Eva, J., Bernacchi, C., 2017. Importance of biophysical effects on climate warming mitigation potential of biofuel crops over the conterminous United States. GCB Bioenergy 9 (3), 577–590.